Hindawi
Mathematical Problems in Engineering
Volume 2019, Article ID 3269108, 19 pages
https://doi.org/10.1155/2019/3269108

Research Article

Analysis of Rigid Body Swing Effect on SCR Response under Top Motion and Wave Action

Bo Zhu,[1,2] **Weiping Huang**,[2] **Zhenwen Sun**,[2] **Xinglong Yao**,[2] **and Juan Liu**[3]

[1]*School of Civil and Ocean Engineering, Jiangsu Ocean University, Lianyungang 222005, China*
[2]*Shandong Key Laboratory of Ocean Engineering, Ocean University of China, Qingdao 266071, China*
[3]*Institute of Civil Engineering, Agriculture University of Qingdao, Qingdao 266009, China*

Correspondence should be addressed to Bo Zhu; beiji_dongjie@qq.com

Received 19 February 2019; Revised 26 May 2019; Accepted 25 June 2019; Published 8 August 2019

Academic Editor: Antonio M. Gonçalves de Lima

Copyright © 2019 Bo Zhu et al. This is an open access article distributed under the Creative Commons Attribution License, which permits unrestricted use, distribution, and reproduction in any medium, provided the original work is properly cited.

The catenary riser such as steel catenary riser (SCR), under wave action or current action, shows a kind of rotation that acts as a rigid body along a similarly fixed axis of oscillation determined by the varying suspension and touch down point, respectively. The characteristics of acceleration of catenary riser influenced by rigid body swing integrity backwards and forwards (RBSIBF) in cross direction cannot be neglected. Based on the large deflection slender beam model, top motion of x direction, RBSIBF, and wave force model, this manuscript studies and explains effect of RBSIBF in cross direction (z direction) on riser in quantitative and qualitative perspectives. The rigid body wiggle effect can be considered by amplitude-value multiplication with the safety factor of 1.2. The calculation shows that, in terms of the overall motion pattern, the motion response in the xy plane develops gradually from the narrow amplitude wiggle in in-line direction of top region to narrow amplitude wiggle in vertical direction of bottom area. Wave load is the main effect load in cross-flow direction. Along the depth increase, the acceleration amplitude of the top hanging point area is maximum, and the amplitude decreases most strongly or violently. With the decrease of case amplitude, the structural acceleration responses of node 10th to 80th significantly reduced by about 30% and the corresponding of node 140th to 200th increased by about 15%. The most influential point of RBSIBF on acceleration is node 200th with an influence level of about 20%. When the structure mainly rotates in the xz plane, rigid body wiggle and swing are positively correlated with rotation vector diameter. The rigid body wiggle and swing increase acceleration of structure. In the rotational yz plane of the structure, rigid body wiggle and swing reduce acceleration response.

1. Introduction

Recent years, offshore oil and gas exploitation has moved gradually to deep water because of the rapid increasing of oil and gas discovery in these areas, which makes a most promising direction of oil and gas industry. More and more equipment has been manufactured to provide support for offshore oil and gas development. Steel catenary riser (SCR) is key equipment used in production of oil and gas. It is most used for the floating offshore platform to provide connection channel between the surface equipment and the underwater wellhead. Since its first application in offshore field in 1994, SCR has been widely applied in varied water depth, which has brought significant economic benefits. Steel catenary riser is usually suspended outside the platform, and the response of SCR is significantly affected by the platform motion. In this paper, the structure is mainly subjected to wave loads, RBSIBF, platform movement, etc. In 3D space, there is vertical interaction between wave force in the bending plane and RBSIBF out of bending plane (in the rotation plane), which makes response of movement turn into a relatively complex random process.

Many scholars have made profound study on the structure and response of SCR. The initial research of SCR mainly includes the joint development plan of 2H offshore engineering "deep sea environment steel riser" in 1997, the joint development plan of the integral analysis of the riser-seabed interaction model industry in 1999, and the mathematical model of the steel catenary riser developed by the University of Sao Paulo in Brazil and Petrobras. In terms

of applications, more than 20 software programs including Deeplines, Flexcom, and Orcaflex have been developed for time domain analysis, frequency domain analysis, wave and vortex-induced vibration fatigue analysis, and installation analysis [1].

Younes Komachi et al. [2] simulated vortex-induced vibration (VIV), structure 3D dynamic response, and stress fatigue ratio by using wake oscillator model and Newmark-β method. Niaz B et al. [3] studied VIV with two-directional RANS model when mass damping is relatively weak. They considered that the locking interval had a larger amplitude and a larger range of drag force coefficients at the reduced velocity of 2-16 to some extent. Vamshikrishna, Domala, and Rajiv Sharma [4] studied and analyzed the vortex-induced vibration response of top tension riser, steel catenary riser, and steel catenary riser with platform motion using experimental methods. Z.Y.Pand et al. [5] studied VIV with RANS model when mass damping is relatively weak. They explained the development of 2P model in detail to some extent. Keum-shik Hong and Umer Hameed Shah [6] analyzed the stability and fatigue of riser by comparing theory and experiment. Euler Bernoulli was used to set up the equations for marine load and ship motion. Hal-jamal et al. [7] used the two-dimensional LES method to calculate the self-excited VIV response of cylinder with Dirichlet-Neuman output boundary conditions. Feras k. Alfosail et al. [8] used state space method to solve self-vibration and riser's buckling load. Liyes Aguedal et al. [9] used LES method to research three-dimensional cylinder VIV. It showed that when the Reynolds number is 3900 and the rotation speed is 0.5-2.0 rad/s, the dimensionless load frequency is 0-8. Wenwu Yang et al. [10] researched nonlinear model and suggested that the natural frequency, maximum displacement and stress of the structure were significantly affected by the Kelvin Voigt viscoelasticity coefficient. MinLou et al. [11] considered the riser's vibration boundary with experimental study, and the study showed that the VIV response of the riser with series and parallel arrangement was significantly reduced. ZhuangKang et al. [12] studied submerged cylinder's VIV phenomenon which is anchored at bottom in uniform flow and studied VIM phenomenon of 6-dof marine structure by using different mass ratios. Xiaohui Wang et al. [13] used two-phase flow and acoustic model to describe the acoustic transmission phenomenon of gas entering into or existing in the riser. They used HHT based acoustic detection for well control and gas detection. F.J.H.uera-huarte et al. [14] tested cylinder which has small quality and obvious flexibility, showing that when the mass ratio is lowest, the amplitude reached 3m, and the drag coefficient exceeded 3. Yongli Hu et al. [15] studied the control equation of different length of riser in the process of underwater tree installation using the Keller-box method. The method is useful for installation issue, and displacement of the top of the riser and underwater tree should be calculated. Narakorn Srinil et al. [16] studied vortex-induced vibration at two direction flow velocities in the plane and out of the curved riser and concluded that the maximum (minimum) response occurred in the case of vertical flow. M.M.Cicolin [17] studied the cylindrical vortex-induced response in low mass and damping using the flexible lateral line structure, and the Ventilated Trousers (VT) can make the response reduced by 40% superior compared with other ways.

From 2013 to 2014, LIU Juan proposed VIV in transverse swing plane considering the rigid body rotation. The rigid body oscillation was realized on Cable3D for the first time in the form of inertial force and hydrodynamic damping. From 2017 to 2018, Fu Xuepeng verified the rigid body motion mode of the steel catenary riser with the form of experiment and solved the rigid body motion frequency for the first time in the way of theoretical formula. Yao Xinglong used Cable3D to conduct secondary development in Cable3D on the basis of experimental analysis, considering vortex-induced vibration, top platform, bottom soil, wave load, fatigue calculation, and other contents. The phenomenon of rigid body oscillation is studied comprehensively. After nearly five years of development, RBSIBF has accumulated a solid foundation in terms of concept generation, programming, experimental verification, and influencing factors, which cannot be separated from the careful guidance of Professor Huang Weiping.

As can be seen from above, the study of SCR mainly concentrated on the calculation of reactions with wave and current action and characteristics of structural reactions under RBSIBF action is rarely involved. In this paper, the deep water linear wave and simple harmonic motion of the platform are used to simulate the actual sea conditions. Rigid body oscillation is superimposed on the response calculation of structural acceleration and frequency. The computational model in this paper is taken from Exxon Mobil (Exxon) Diana [18]. The loads such as wave, top motion of in-line direction, and RBSIBF act on the structure. The following response problems need to be solved:

(1) The effect of RBSIBF on structural response needs to be studied. Most commercial programs cannot directly simulate rigid body motion. The direct simulation by specialized program Cable3D also takes more time for calculations. It is suitable for structural design considering the effect of RBSIBF in a certain safety coefficient.

(2) The load of SCR is wave, in-line top motion and rigid body oscillation. Structure is subjected to x and z direction loads. Sum frequency and difference frequency phenomenon exist in x direction wave load and top motion. The structural acceleration should be verified and compared with the Lissajous' figures; the value of acceleration response is also needed.

(3) The structural response is affected by wave frequency, x direction motion frequency, RBSIBF frequency, and structural natural vibration frequency. The characteristics of structural frequency response need to be studied. Meanwhile, simple and accurate formula to simulate the frequency of rigid body oscillation is rare.

2. SCR Numerical Integrated Model

The SCR numerical integrated model refers to the integration of specific solution system by means of subprogram model for Cable3D simulation. It comes from the superposition and expansion of the load term of the basic equation.

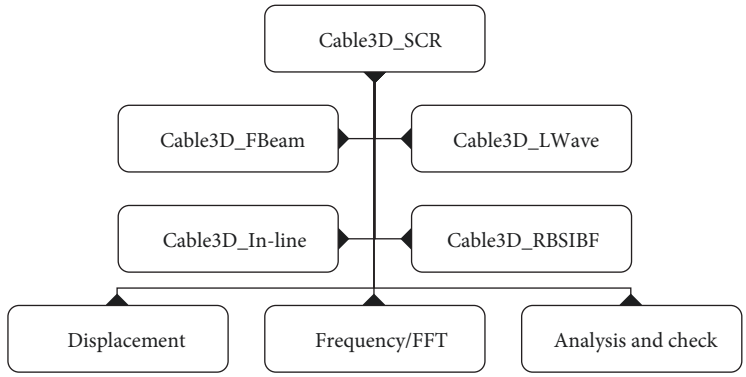

Figure 1: Calculation process of structural model.

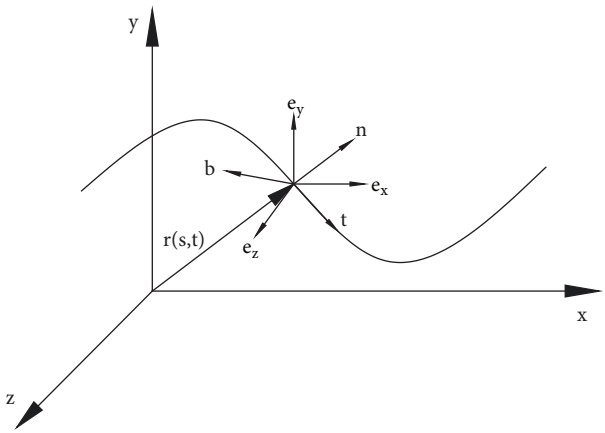

Figure 2: The curvilinear coordinate system of beams.

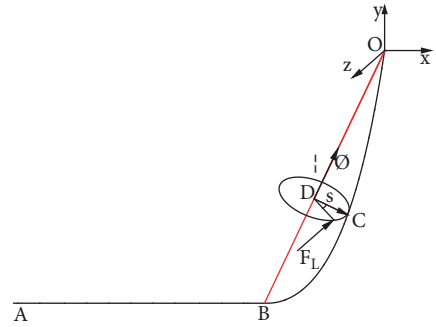

Figure 3: Swing of catenary system [19].

2.1. SCR Numerical Model. SCR numerical model [19] is the basic equation to calculate the response of structure acceleration, velocity and so on. The basic control equation of riser motion is derived with beam balance, large deflection, and vibration expression. In this derivation, based on the expression of load term and mass term, the equation is deduced step by step.

Cable3D was developed by Chen, Texas A&M University of America. It is a response program for solving SCR complex response such as platform motion, fluid-solid coupling, pipe-soil interaction, RBSIBF, and so on. The integration of multiple effects can simulate these complicated phenomena. The model used in this paper is shown in Figures 1–3.

The SCR numerical calculation adopts the large deflection slender beam model. This model is the foundation of Cable3D simulation and expansion. The load model component of the SCR is used to extend the mathematical model for Cable3D development. The iterative process, which is the basis of model calculation and update, is often encountered in RBSIBF iterative simulation.

The integral coordinate system of the riser is shown in Figure 2 [19]. In the coordinate, arc length s and time t are the independent variables of displacement $\vec{r}(s,t)$. For the curvilinear coordinate system, the unit vector is expressed as $\vec{e}_x$, $\vec{e}_y$, and $\vec{e}_z$, while the normal, subnormal, and tangent unit vectors are expressed as $\vec{n}$, $\vec{b}$, and $\vec{t}$.

According to momentum and other theories related to momentum theory, beam formula with length ds is gained.

$$\frac{df}{ds} + q = \rho \frac{d^2 r}{dt^2} \tag{1}$$

$$\frac{d\widetilde{m}}{ds} + \frac{dr}{ds} \times f + m = 0 \tag{2}$$

In the formulas, f is internal force; q is distribution force; ρ is density; $\widetilde{m}$ is internal moment; m is external torque. The moment solved with Bernoulli-Euler is gained:

$$\widetilde{m} = B\frac{d^3 r}{ds^3} + H\frac{dr}{ds} \tag{3}$$

Take the derivative of $\widetilde{m}$:

$$\frac{d\widetilde{m}}{ds} = B\frac{d^4 r}{ds^4} + \frac{drdH}{dsds} + H\frac{d^2 r}{ds^2} \tag{4}$$

where B is bending stiffness and H is torque. Assume that torque is not considered; the internal moment is substituted in (2):

$$f = \lambda \frac{dr}{ds} - B\frac{d^3 r}{ds^3} \tag{5}$$

where λ is the Lagrangian operator. $\lambda = T - B\kappa^2$, T is tension of riser, B is bending, and κ is curvature.

Substitute (5) into (1); motion formula considering the flexibility can be written as

$$\rho\frac{d^2r}{dt^2} + B\frac{d^4r}{ds^4} - \lambda\frac{d^2r}{ds^2} = q \tag{6}$$

Unit length gravity of the riser is as follows:

$$q_t(s,t) = -\rho_t A_t g \tag{7}$$

Inertia force is as follows:

$$\begin{aligned} q_f^I(s,t) &= \rho_f A_f C_{Mn}\left(\frac{du}{dt} - \frac{d^2r}{dt^2}\right) \\ &\quad + \rho_f A_f C_{Mt}\left(\frac{du}{dt} - \frac{d^2r}{dt^2}\right) \end{aligned} \tag{8}$$

Drag force is as follows:

$$\begin{aligned} q_f^D(s,t) &= \frac{1}{2}\rho_f D_f C_{Dn}\left(u - \frac{dr}{dt}\right)\left|u - \frac{dr}{dt}\right| \\ &\quad + \frac{1}{2}\rho_f D_f C_{Dt}\left(u - \frac{dr}{dt}\right)\left|u - \frac{dr}{dt}\right| \end{aligned} \tag{9}$$

In the formula, C_{Mn} and C_{Mt} are normal additional mass factor and tangential factor, respectively; C_{Dn} and C_{Dt} are drag coefficient in normal direction and in tangential direction, respectively; ρ_t is pipe diameter density; ρ_f is sea water density; ρ_i is fluid density in the pipe; A_t is cross-section area; A_i is inner diameter area; A_i is outside diameter area.

F-K force outside the riser is as follows:

$$q_f^{F-K}(s,t) = \rho_f A_f g + P_f A_f\frac{d^2r}{ds^2} + \rho_f A_f\frac{du}{dt} \tag{10}$$

F-K force in riser is as follows:

$$q_i^{F-K}(s,t) = \rho_i A_i g + P_i A_i\frac{d^2r}{ds^2} \tag{11}$$

In the formula, D_t is external diameter; u and $\dot{u}$ are velocity of seawater and acceleration of seawater, respectively. P_f is seawater pressure. P_i is the fluid pressure in the pipe. After the momentum moment calculation of the beam balance equation, the load replacement of motion formula, and consolidation of the load term, the basic calculation formula is as follows:

$$M\frac{d^2r}{dt^2}(s,t) = \lambda\frac{d^2r}{ds^2}(s,t) - B\frac{d^4r}{ds^4}(s,t) + q \tag{12}$$

In the formula, M is the mass matrix:

$$M = f\left(q_f^I, q_f^{F-K}, q_i^{F-K}\right) \tag{13}$$

q is load matrix:

$$q = f\left(q_t, q_f^I, q_f^{F-K}, q_i^{F-K}, q_f^D\right) \tag{14}$$

λ is the Lagrangian operator:

$$\widetilde{\lambda} = \left(T + P_f A_f - P_i A_i\right) - B\kappa^2 \tag{15}$$

In the formula, T is tension matrix.

The foundation of structural numerical simulation is the solution of response to structural displacement by the above formula [1]. The basic model of SCR solution includes gravity, inertial term, tension, and Fredric-Krylov term. Under given parameters, mass term, load term, and Lagrangian operator matrix of the structure develop the basic solution conditions.

2.2. LOAD Numerical Model. The extension of numerical model is classified as LOAD numerical model. The expansion calculation is usually carried out in the form of load terms.

2.2.1. LOAD-SCR Integral Oscillation. Main goal for SCR rigid body oscillation is the simulation of SCR swing phenomenon around axis OB caused by deep water wave, water flow, and other loads.

According to the basic formula [19], rotation formula is gained:

$$(m + m_a)s^2\frac{d^2a_r}{dt^2} + c_a s^2\frac{da_r}{dt} = q_r \tag{16}$$

$$q_r = q_z\sqrt{s_1^2 + s_2^2} + q_x\omega_2 s_3 - mg\omega_1 s a_r \tag{17}$$

In the formula, m and m_a are riser mass and riser additional mass; c_a is riser additional damping; q is riser load; a_r, $\dot{a}_r$, and $\ddot{a}_r$ are angular displacement and its first and second derivatives coupling riser's RBSIBF; s_1, s_2, and s_3 are radius vector components in in-line, vertical, and transverse directions; ω_1, ω_2, and ω_3 s_3 are rotation vector components in in-line, vertical, and transverse directions. The above formula considers the radius, angular velocity, angular acceleration, angular displacement, etc.

It can be expanded it in three directions

$$\begin{aligned} &(m + m_a)\left(\frac{d^2u_b}{dt^2} + \frac{d^2u_r}{dt^2}\right) + (c + c_a)\frac{du_b}{dt} \\ &\quad = q_x - c_a\frac{du_r}{dt} - ku_b \end{aligned} \tag{18}$$

$$\begin{aligned} &(m + m_a)\left(\frac{d^2v_b}{dt^2} + \frac{d^2v_r}{dt^2}\right) + (c + c_a)\frac{dv_b}{dt} \\ &\quad = q_y - mg - c_a\frac{dv_r}{dt} - kv_b \end{aligned} \tag{19}$$

$$\begin{aligned} &(m + m_a)\left(\frac{d^2w_b}{dt^2} + \frac{d^2w_r}{dt^2}\right) + (c + c_a)\frac{dw_b}{dt} \\ &\quad = q_z - c_a\frac{dw_r}{dt} - kw_b \end{aligned} \tag{20}$$

where u_b, v_b, w_b, $\dot{u}_b$, $\dot{v}_b$, $\dot{w}_b$, $\ddot{u}_b$, $\ddot{v}_b$, $\ddot{w}_b$ represent components of displacement and its first and second derivatives considering the bending in in-line, vertical, and transverse

directions; $u_r, v_r, w_r, \dot{u}_r, \dot{v}_r, \dot{w}_r, \ddot{u}_r, \ddot{v}_r$ represent components of displacement and its first and second derivatives considering the RBSIBF in in-line, vertical, and transverse directions;

$$\begin{aligned} \overrightarrow{v}_r &= \dot{a}_r \left(\overrightarrow{c} \times \overrightarrow{s}\right), \\ \overrightarrow{a}_r &= \ddot{a}_r \left(\overrightarrow{c} \times \overrightarrow{s}\right) \end{aligned} \tag{21}$$

It can be expanded it in three directions

$$\begin{aligned} \dot{u}_r &= \frac{da_r}{dt}\left(\omega_2 s_3 - \omega_3 s_2\right), \\ \dot{v}_r &= \frac{da_r}{dt}\left(\omega_3 s_1 - \omega_1 s_3\right) \\ \dot{w}_r &= \frac{da_r}{dt}\left(\omega_1 s_2 - \omega_2 s_1\right) \end{aligned} \tag{22}$$

$$\begin{aligned} \ddot{u}_r &= \frac{d^2 a_r}{dt^2}\left(\omega_2 s_3 - \omega_3 s_2\right) \\ \ddot{v}_r &= \frac{d^2 a_r}{dt^2}\left(\omega_3 s_1 - \omega_1 s_3\right) \\ \ddot{w}_r &= \frac{d^2 a_r}{dt^2}\left(\omega_1 s_2 - \omega_2 s_1\right) \end{aligned} \tag{23}$$

2.2.2. LOAD-SCR Wave Model. The solution of interaction between structure and wave is the main target of SCR wave model. The relative velocity and acceleration term are substituted into the Morison equation to replace the original formula. The linear wave velocity potential function in deep water is substituted into the equation

$$\phi_0 = \frac{gA}{\sigma} e^{kz} \sin\left(kx - \sigma t\right) \tag{24}$$

$$\xi_0 = -Ae^{kz} \sin\theta \tag{25}$$

$$\varsigma_0 = Ae^{kz} \cos\theta \tag{26}$$

$$\begin{aligned} f_H = {} & \frac{1}{2} C_D \rho A \left(\frac{du}{dr} - \frac{dr}{dt}\right)\left|\frac{du}{dr} - \frac{dr}{dt}\right| \\ & + C_M \rho \frac{\pi D^2}{4}\frac{\partial u}{\partial t} - C_m \rho \frac{\pi D^2}{4}\frac{d^2 r}{dt^2} \end{aligned} \tag{27}$$

In the formula, A, $\overline{V}_0$ are riser property; C_m, C_M, C_D are hydrodynamic coefficient; u_x and u_x^t are water quality point horizontal velocity and acceleration [1, 19]. The above formula considers the inertial force term, drag force term, and additional mass term.

2.2.3. LOAD-SCR X Movement. The cross-flow motion of the platform adopts the x motion simulation of the top end point of SCR [1, 19].

Top motion calculation is as follows:

$$F_L = k_1 A \cos\omega_s t \tag{28}$$

The formula considers the amplitude of the interaction between waves and solids:

$$A_r = A - r \tag{29}$$

The top model is

$$Q_x = k_1 A_r \cos\omega_s t \tag{30}$$

where A, k_1 are amplitude of platform components and its scale factor; ω_s is platform vibration frequency.

$$\begin{aligned} M\frac{d^2 r}{dt^2} = {} & \lambda \frac{d^2 r}{ds^2} - B\frac{d^4 r}{ds^4} + q + mg - \left(m + m_a\right)\frac{d^2 r_r}{dt^2} \\ & - c_a \frac{dr_r}{dt} + f_H + Q_x \end{aligned} \tag{31}$$

In the formula, the calculated value of the load caused by the x direction motion is Q_x. For formula (31), the frequency input of the right end of the load term affects the load response frequency. The complex and stochastic characteristics of the structure response also come from the input of different frequency and amplitude load components.

2.3. Numerical Model Calculation. The hanging point's fixed constraint and the in-line motion is modified and added in the calculation document. During this part, the SCR beam considering large deflection and its load numerical term including RBSIBF, x direction motion, and wave load are provided.

Based on the numerical model, Cable3D simulates reactions affected by in-line wave and platform motion at hanging point. Cable3D-Vswing calculates the response affected by in-line wave and platform motion at hanging point and RBSIBF. The difference in the program is whether the structural response takes into account the effect of RBSIBF.

Structural reaction characteristics need to be analyzed from two aspects: along water depth and considering RBSIBF or not. Finally, effect of RBSIBF is evaluated through a certain factor considering the safety.

3. SCR Design Scheme Parameters

SPAR+SCR+subsea tree is a widely used mode in offshore oil exploitation, which is also applied in Exxon Mobil Diana oil field.

In order to adapt to the new design scheme, the structure length and other parameters are adjusted accordingly. The adjustment method can be simply carried out according to the original structure length multiplied by the ratio of current depth and origin depth. The structure is influenced by RBSIBF within a limit. It is effective for the design if effect of RBSIBF can be taken into account through a certain factor.

3.1. Engineering Scheme. The water depth is 1100m. The wave period is 8.6s and the wave height is 3.5m. The density of crude oil for transportation is 865kg/m^3, the normal working speed in the pipe is 1-2m/s, and it may be empty pipe under some other cases with a design life of 20 years. Seawater

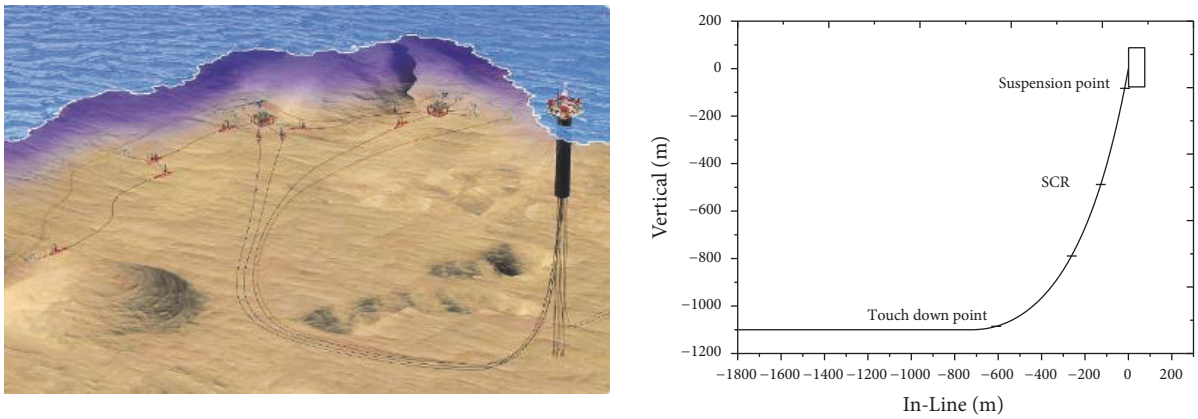

Figure 4: Oilfield environment and static schematic diagram of SCR.

density out of riser is 1025kg/m^3, and the velocity is not calculated in this paper. In addition to the central well designed to accommodate 8 TTRs, SCR is also needed. The total length of SCR is 2400m, the anchor position is around 1800m, and the contact position is around 700m. The top of the SCR is connected to the soft cabin through flexible joints. The base plate connection is used at the bottom. Exxon Mobil Diana oil field is shown in Figure 4, and its working tree pressure is 10000psi. The name rotating stiffness of main parameters of flexible joint is from 93.994 kN·m/deg to 11.988 kN·m/deg and the angle is from 0° to 20°. The SCR structure contains five layers as shown in Table 1.

3.2. Numerical Simulation Parameters. The wave loads in the in-line direction adopt deep water linear wave with frequency of 0.11622Hz. Table 2 gives some parameters. Only the harmonic motion in in-line direction applied on hanging point is calculated by numerical simulation, as shown in the Table 3. And Table 4 are the frequencies. The simulation of the structure adopts 400 nodes, 399 beam elements with large deflection and shape expression to solve the reactions. The interaction between the structure and the seabed is calculated by using a formula proportional to the depth. The quadratic Hermite function is used for the mass, stiffness, Lagrangian operator and external load matrix. The 3D beam element model is calculated by finite element method. The spring stiffness of the vertex and anchor point is 0.1E12Pa and the bottom friction coefficient is 0.2. The calculation time is 1000s, and the step length is 0.1s. The incremental iteration factors are 0.7. The error is 0.1E-5, and iteration step is 40.

3.3. Frequency Resonance and High-Low Analysis. The structural response can be decomposed into the superposition of different loads by a specific method. In terms of frequency, different load frequencies have obvious effects on the structural response. The reaction is solved to obtain the amplitude and phase graph, so as to find the main frequency and other influence frequencies.

The frequency with in-line wave is 0.11622Hz, and in-line platform movement frequency is from 0.093Hz to 0.111Hz. The value of first order frequency of the structural bending vibration obtained by Vandiver method is 0.016Hz. The frequency value of RBSIBF obtained through Rayleigh formula is 0.029Hz [19].

Structural frequency is compared as follows: wave frequency > x direction motion frequency > RBSIBF frequency > structure bending frequency (first order).

Rayleigh method [20] solves the frequency of RBSIBF:

$$T = \frac{1}{2}\sum_i m_i \dot{x}_i^2 = \frac{1}{2}\left(\frac{1}{3}m_1 l^2 + \frac{1}{3}m_a l^2 + m_2 l^2\right)\omega^2 A^2 \cos^2\theta \tag{32}$$

$$V = \frac{1}{2}\sum_i k_i x_i^2 = \frac{1}{2}\left(kl^2\right)A^2 \sin^2\theta = \frac{1}{2}\left(\frac{1}{2}m_1 gl + \frac{1}{2}m_a gl + m_2 gl\right)A^2 \sin^2\theta \tag{33}$$

$$T_{\max} = V_{\max} \tag{34}$$

$$\omega = \sqrt{\frac{1/2m_1 gl + 1/2m_a gl + m_2 gl}{1/3m_1 l^2 + 1/3m_a l^2 + m_2 l^2}} \tag{35}$$

In the formula, ω is angular frequency; k_1 is restoration stiffness; x is structural displacement; A is swing magnitude; l is swing length; m_1 is swing mass; m_2 is bottom mass summation; m_a is bottom mass concentration.

The bending vibration method [20] solves the natural vibration frequency:

$$\omega = (n\pi)^2\sqrt{\frac{EI}{ml^4}}, \quad n = 1, 2, \cdots, \infty \tag{36}$$

where ω is angular frequency; EI is stiffness; m is structural mass; l is structural length.

3.4. 3D Response Diagram of Structure Particle Acceleration. When affected by orthogonal loads such as in-line wave and RBSIBF in rotation plane, the acceleration responses of the structural nodes can be obtained. By plotting the 10th,

Table 1: Pipe functional structure.

Layers	Layers load	layer Properties	Layer quality(kg/m^3)
Bearing layer	Bearing Pressure, Bending, stretching, etc	Steel	7.85E03
Anticorrosion layer	Prevent osmotic corrosion	Epoxy resin	1.44E03
Bonding layer	Inter-layer bonding	Propathene	9.80E02
Heat preservation and insulation layer	Keep the temperature for Crude oil delivery	Foam polypropylene	8.00E02
External protection layer	Prevent seabed damage	Polyethylene	9.00E02

Table 2: SCR parameters [1].

Design Conditions	Value
m(kg/m)	2.9600E02
Buoyancy (N/m)	2.1370E03
D (m)	3.550E-01
d (m)	3.050E-01

Table 3: Motion parameters [19].

Conditions	Amplitude /m	Period /s	Frequency
1	3.00	10.8	0.093
2	2.00	9.90	0.101
3	1.00	9.00	0.111

Table 4: Structural frequencies under load excitation.

Load frequency	Value
Wave(Hz)	0.11622
X motion(Hz)	0.093-0.111
RBSIBF(Hz)	0.029
The natural vibration frequency (Hz)	0.016/0.064/0.144

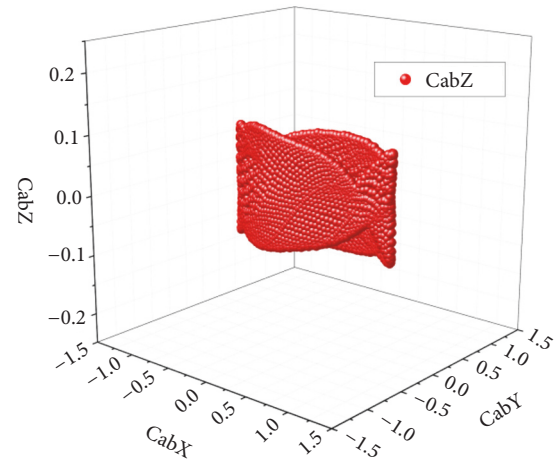

Figure 5: The 10th node acceleration reaction of no RBSIBF.

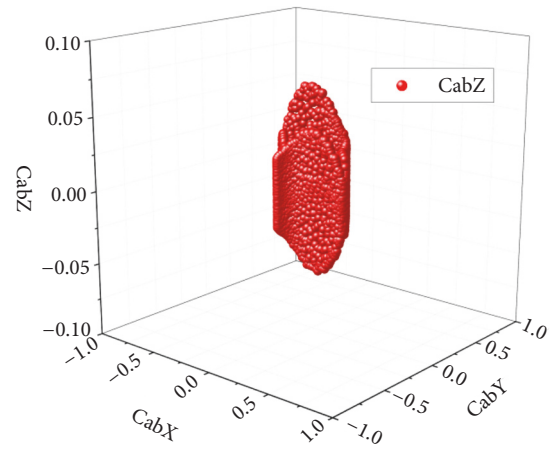

Figure 6: The 80th node acceleration reaction of no RBSIBF.

80th, 140th, and 200th nodes accelerations, the 3D figures of the non-RBSIBF can be presented, as shown in Figures 5–8. Bending plane figures no RBSIBF and with RBSIBF are presented for Figures 9–12.

In terms of horizontal comparison, Figures 5–8 show the three-dimensional structural response graphs of non-RBSIBF structure withstanding wave and in-line motion. Figures 9–12 are the graphs of xy plane. The xy plane is a projection or refraction of the structural response into a plane of the structural x direction (in-line) and y direction (vertical). There is no significant difference between the motion of the two sets of graphs in the plane of forward flow direction and vertical direction. The RBSIBF is not the major influence factors acting on the plane, which can be made out from orthogonal characteristic of RBSIBF and bending vibration. RBSIBF is out-of-plane motion perpendicular to the bending vibration. Except for no significant difference in xy plane, the difference in z direction is the difference in amplitude and curve form of structural response.

Figures 5–8 correspond to 3D acceleration reaction of the 10th-200th nodes, respectively. It is more appropriate to recognize them from the supplement perspective of 2D plane of Figures 9–12. When node number or depth augmenting, motion reaction in the xy plane developed from in-line direction narrow range oscillation of the 10th node to y direction narrow range oscillation of the 200th node.

The response of the 10th node is a narrow range in-line oscillation. 80th node's reaction is a wider range oscillation about 30° deflection from in-line direction. 140th node's reaction is a narrow range eight-lane oscillation about 70° deflection from in-line direction. 200th node's reaction is a wide

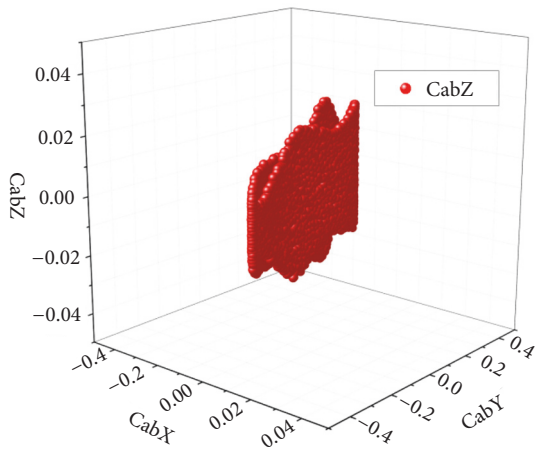

Figure 7: The 140th node acceleration reaction of no RBSIBF.

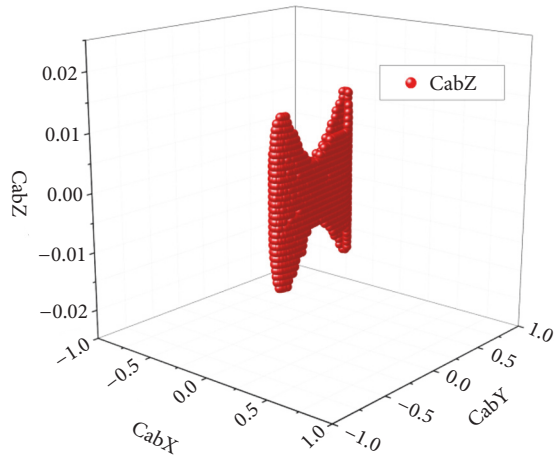

Figure 8: The 200th node acceleration reaction of no RBSIBF.

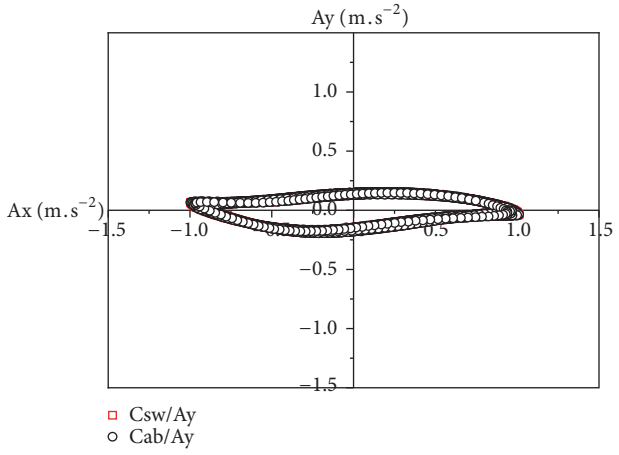

Figure 9: The 10th node acceleration with and without RBSIBF in xy plane.

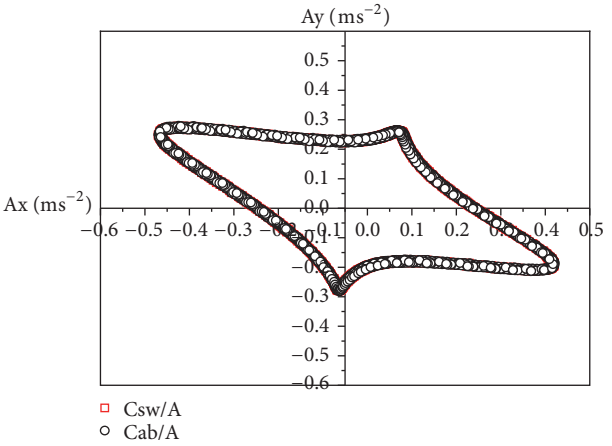

Figure 10: The 80th node acceleration with and without RBSIBF in xy plane.

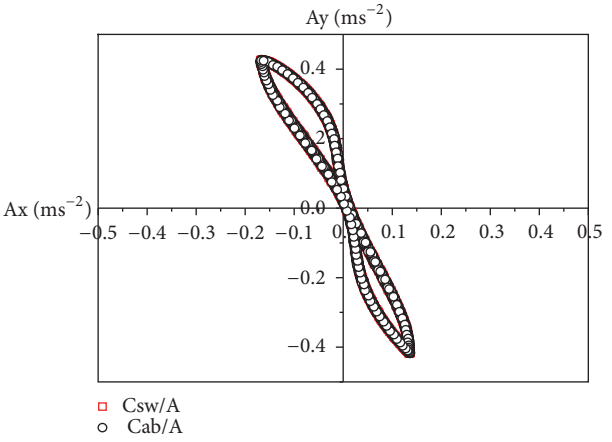

Figure 11: The 140th node acceleration with and without RBSIBF in xy plane.

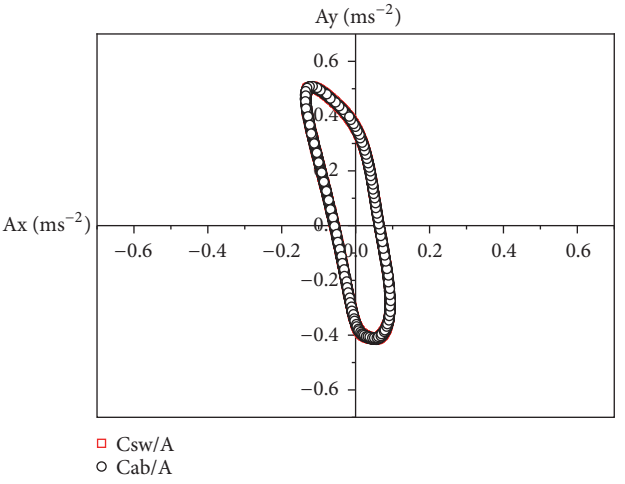

Figure 12: The 200th node acceleration with and without RBSIBF in xy plane.

range eight-lane oscillation about 70° deflection from in-line direction. The swing amplitude gradually decreased; the maximum acceleration of the 10th node is about 1.01247m.s^{-2}. The parameters are shown in Table 5.

As the water depth increases, the xy plane motion of the above structure is mainly excited by the x direction oscillation and gradually transited to the y direction oscillation. The amplitude oscillation attenuation of the upper node had maximum amplitude, maximum deflection angle from the y direction and the most intense activity. When node number augmenting, oscillation amplitude reduces in y direction.

Figures 5–12 helps to understand the structural response of SCR structural particles at different locations from a 3D perspective. This article focuses on the characteristics of acceleration in z direction.

4. SCR Calculation and Analysis

4.1. Analysis of SCR Acceleration

4.1.1. SCR Basic Formula [1].

$$\gamma_{ikm}M_{njm}\ddot{u}_{kj} + \alpha_{ikm}B_m u_{kn} + \beta_{ikm}\widetilde{\lambda}_m u_{kn} = \mu_{im}q_{mn} + f_{in} \tag{37}$$

Formula (37) is essential to simulation of static and dynamic displacement. If term $\ddot{u}_{kj}$ is equal to 0, the above equation becomes the SCR static displacement equation.

$$\alpha_{ikm}B_m u_{kn} + \beta_{ikm}\widetilde{\lambda}_m u_{kn} = \mu_{im}q_{mn} + f_{in} \tag{38}$$

The displacement u and Lagrange $\widetilde{\lambda}$ are calculated by using the following equations iteratively:

$$u_{kn} = u^0_{kn} + \delta u_{kn} \tag{39}$$

$$\widetilde{\lambda}_m = \widetilde{\lambda}^0_m + \delta\widetilde{\lambda}_m \tag{40}$$

Newmark-β method is used to calculate SCR dynamic equation formula (41). If $t = 0$, the dynamic equation is calculated by the following formula:

$$\gamma_{ikm}M^{(0)}_{njm}\ddot{u}^{(0)}_{kj} + \alpha_{ikm}B_m u^{(0)}_{kn} + \beta_{ikm}\widetilde{\lambda}^{(0)}_m u^{(0)}_{kn} = \mu_{im}q^{(0)}_{mn} + f^{(0)}_{in} \tag{41}$$

The initial acceleration $\ddot{u}^{(0)}$ is calculated on the basis of displacement $u^{(0)}$ and Lagrange $\widetilde{\lambda}^0$. Based on the expression at the moment of K-1, the following substitution method is adopted to calculate $u^{(K)}$, $\dot{u}^{(K)}$, $\ddot{u}^{(K)}$, and $\widetilde{\lambda}^{(K)}$ at the moment of K.

$$\ddot{u}^{(K)} = \ddot{u}^{(K-1)} \tag{42}$$

$$\dot{u}^{(K)} = \dot{u}^{(K-1)} + \Delta t\left(1-\gamma\right)\ddot{u}^{(K-1)} + \Delta t^2\beta\ddot{u}^{(K)} \tag{43}$$

$$u^{(K)} = u^{(K-1)} + \Delta t\dot{u}^{(K-1)} + \Delta t^2\left(\frac{1}{2}-\beta\right)\ddot{u}^{(K-1)} + \Delta t^2\beta\ddot{u}^{(K)} \tag{44}$$

$$\widetilde{\lambda}^{(K)} = \widetilde{\lambda}^{(K-1)} \tag{45}$$

The mass and load may be gained through substituting formulas (42)-(45) into the expression (37)-(41) with the numeric value.

The velocity equivalent expression of the structure response is obtained from the SCR displacement response by applying the basic theory of finite element. On this basis, the iterative solution of wave load, the iterative solution formula of RBSIBF, and other structural loads can be calculated. The updates of structural models and other coupled patterns come from these iterative solutions.

4.1.2. The Phenomenon of SCR Structure Lissajous' Figures, Calculation, and Verification. The Lissajous phenomenon of SCR [21, 22] is a stable closed curve formed when loads are orthogonal in horizontal plane. During this paper, RBSIBF and wave coupling top motion are orthogonal to each other in space.

$$y(s,t) = A\cos\left[\omega\left(t-\frac{s}{v}\right)+\varphi\right] \tag{46}$$

$$y = y_1(r_1,t)\overrightarrow{i} + y_2(r_2,t)\overrightarrow{j} \tag{47}$$

$$x = A_1\cos\left(2\pi n_1 t + \varphi_1\right) \tag{48}$$

$$y = A_2\cos\left(2\pi n_2 t + \varphi_2\right) \tag{49}$$

$$2\pi n_1 t + \varphi_1 + 2k\pi = \pm\arccos\frac{x}{A_1} \tag{50}$$

$$2\pi n_2 t + \varphi_2 + 2m\pi = \pm\arccos\frac{y}{A_2} \tag{51}$$

$n_1/n_2 = m_1/m_2$ (m_1 and m_2-integer of mutual quality). And the trajectory equation is

$$\cos\left(m_1\arccos\frac{y}{A_2} \pm m_2\arccos\frac{x}{A_1}\right) = \cos\left(m_1\varphi_2 - m_2\varphi_1\right) \tag{52}$$

The Lissajous shape is determined by the frequency ratio m_1/m_2 and $\cos(m_1\varphi_2 - m_2\varphi_1)$.

During this manuscript, wave frequency which is in the in-line direction is 0.11622Hz. Top platform sway frequency in case 1 is 0.093Hz. The simulated frequency is 0.09Hz and 0.12Hz with proportion from 3:4 to 4:5.

The reaction curve caused by wave lacks check rules similar to VIV. To some extent, Lissajous phenomenon is a rough qualitative check. When loads mutually vertical and proportion ratio integer, the existing literatures can provide the function of curve verification. If the amplitude ratio is not 1, the graph needs some postprocessing in both directions.

If the amplitude of structural response is not 1:1, it can still be checked by Lissajous figure through horizontal and vertical coordinate system adjustments. In in-line direction, the structure is affected by wave and top motion. There should be response features of sum frequency 2ω, difference frequency, and haploid frequency ω in the response graph. The wave frequency is 0.11622Hz and top motion frequency is 0.093-0.111Hz. They will generate nearly twice the frequency,

Table 5: Amplitude and angle from in-line direction axis of xy plane oscillation curve.

Node	Cab Amplitude (m.s^{-2})	Cab Angle (°)	Csw Amplitude (m.s^{-2})	Cab Angle (°)
10th	1.01247	-1.754559	1.01347	-1.75282
80th	0.53497	-30.06370	0.53509	-29.43941
140th	0.45850	-68.63950	0.45830	-68.36110
200th	0.52147	-76.47008	0.52121	-76.12373

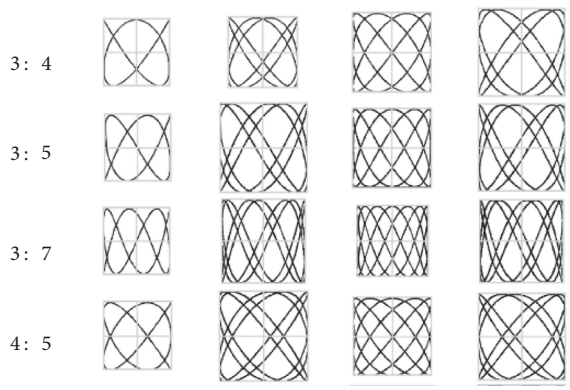

Figure 13: Lissajous graph table.

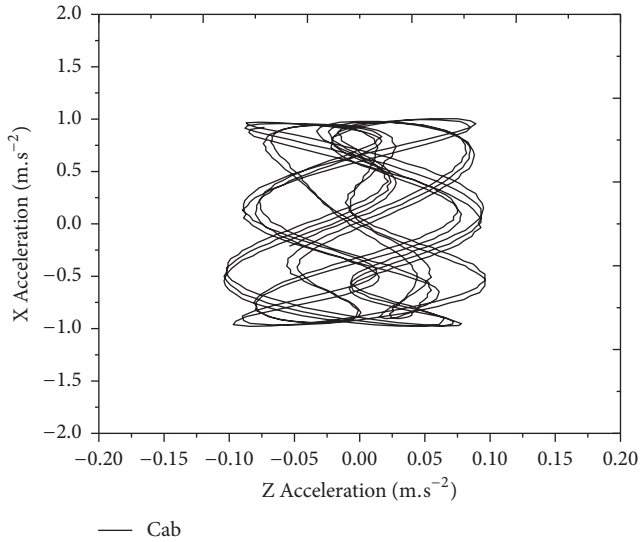

Figure 14: Lissajous figure of the 10th node in zx plane.

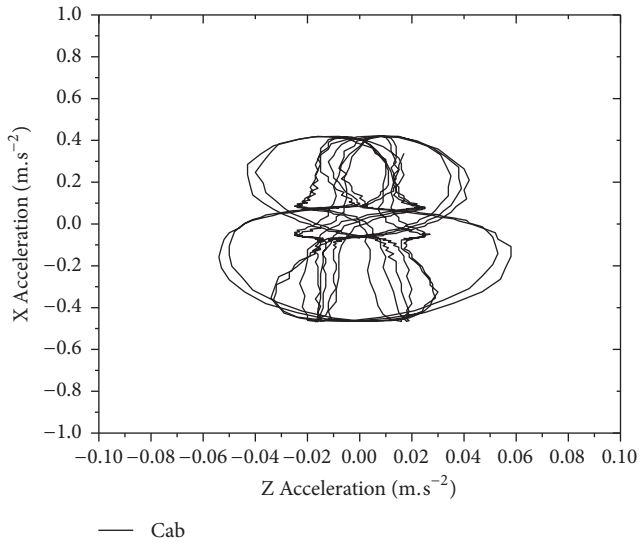

Figure 15: Lissajous figure of the 80th node in zx plane.

and the haploid and difference frequency will also generate response along direction.

For case 1, the response of node 10th-200th in the xz plane is studied through calculation by Cable3D and comparison to Lissajous figures, and the structural response is shown in Figures 14–17.

For node 10th-200th, there are structural responses with frequency ratios of 1:2, 3:4 or 4:5. For the large profile, the structural response path is shaped like Figure 8, which are more explicit in Figures 15 and 16. Figure 8 oscillations represent the sum frequency by wave and top motion frequency in in-line direction. The frequency ratio is close to 1:2.

In Figure 8 oscillations, there are inner oscillations with frequency ratio of 3:4 or 4:5. The figure is similar to the oscillation in Figure 4 of the frequency ratio of 3:4, as shown in Figure 13. The figure is also similar to the oscillation in Figure 2 of the frequency ratio of 4:5, as shown in Figure 13.

Under the characteristics of frequency ratio 1:2, the internal frequency ratio of 3:4 oscillation has a certain similarity of up and down oscillation, which can be understood as the difference frequency characteristic of the structure in Figures 15 and 16. The structure difference frequency represents that the structure has certain motion when the frequency of wave and top motion structure is close to each other. This motion can be understood as the phase difference of the structure or the oscillation of the frequency ratio 3:4.

In terms of the deformation degree of response, the structural response is strengthening, and the difference between curve and standard is obvious. It shows that the complexity of bottom motion is increasing when node number augmenting. Results influenced by wave can be relative easily checked from the above phenomenon.

4.1.3. SCR Acceleration Response Analysis [23, 24]. The above response characteristics in xy plane and zx plane are the response of riser vibration and verification. This paper mainly focuses on response in the z direction (transverse direction). Transverse reaction simulated is based on the angle perpendicular to the bending plane, which is a key problem for structural vibration system. The structure response of the

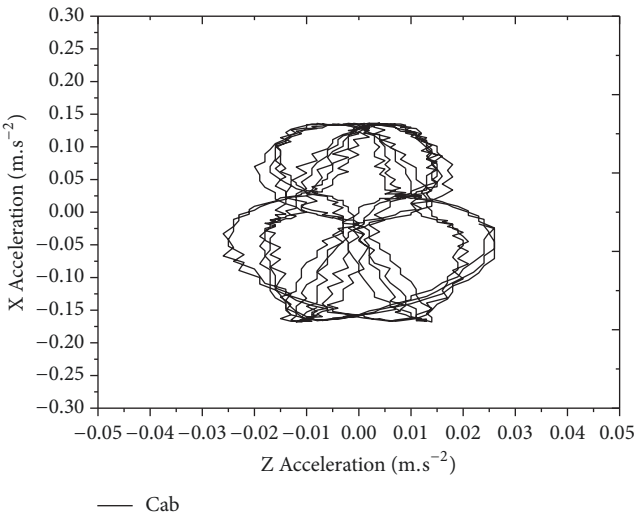

Figure 16: Lissajous figure of the 140th node in zx plane.

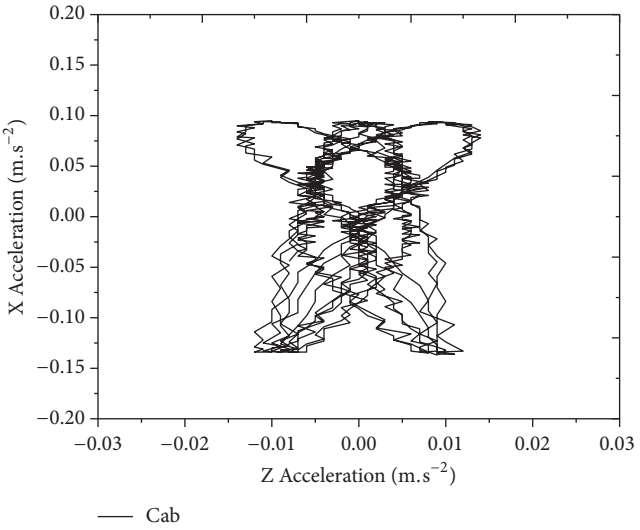

Figure 17: Lissajous figure of the 200th node in zx plane.

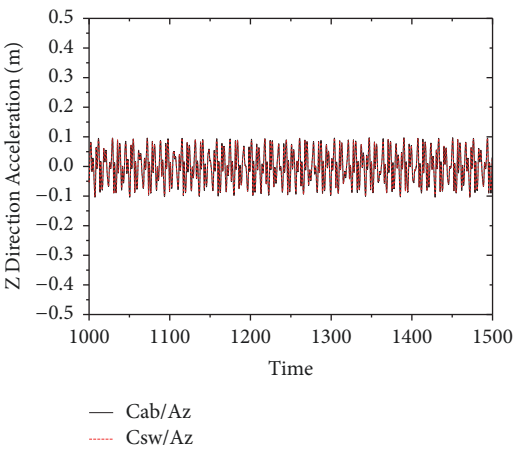

Figure 18: 10th acceleration reaction of case 1.

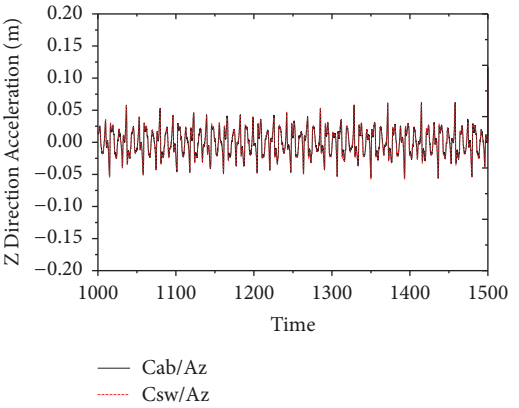

Figure 19: 80th acceleration reaction of case 1.

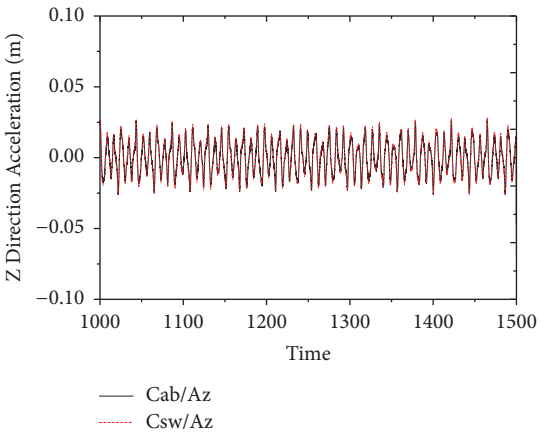

Figure 20: 140th acceleration reaction of case 1.

transverse flow direction includes the response caused by VIV, the response caused by the transverse flow load, and the response caused by the RBSIBF.

The response under the influence of vortex-induced vibration and top in-line motion is often mentioned in research articles while the structural reaction considering wave, in-line platform motion and RBSIBF is rarely studied. The study of cross-flow acceleration response is mainly carried out by applying linear wave, linear top motion, and RBSIBF. The case 1 10th-200th responses are presented in Figures 18–21. Structural transverse maximum reaction and relative reduction along water depth are presented in Tables 6 and 7.

The effect of wave, top x motion, and RBSIBF on the structure can be a simple linear superposition process.

$$\overrightarrow{R}_{cab} = \overrightarrow{R}_{wave} + \overrightarrow{R}_{x} \tag{53}$$

$$\overrightarrow{R}_{csw} = \overrightarrow{R}_{wave} + \overrightarrow{R}_{x} + \overrightarrow{R}_{rbs} \tag{54}$$

$$\eta = \frac{\left(\left|\overrightarrow{R}_{csw}\right| - \left|\overrightarrow{R}_{cab}\right|\right)}{\left|\overrightarrow{R}_{cab}\right|} \tag{55}$$

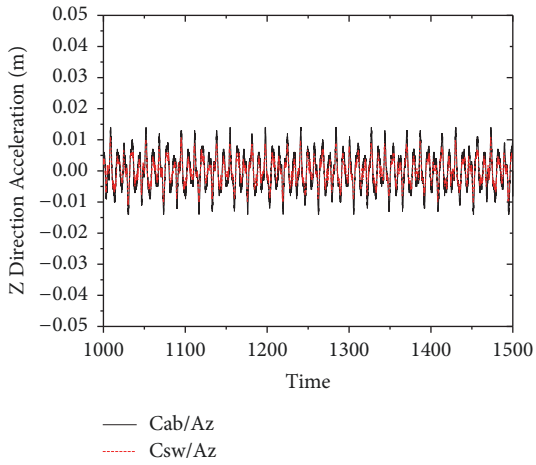

Figure 21: 200th acceleration reaction of case 1.

Table 6: The calculated value of acceleration of nodes in each case.

Cas.	Node	Cab (m/s^2)	Csw (m/s^2)	η
Cas.1	10	9.70E-02	9.60E-02	-0.01
Cas.1	80	6.20E-02	6.30E-02	0.02
Cas.1	140	2.70E-02	2.80E-02	0.04
Cas.1	200	1.40E-02	1.10E-02	-0.21
Cas.2	10	8.70E-02	8.60E-02	-0.01
Cas.2	80	6.10E-02	6.30E-02	0.03
Cas.2	140	3.00E-02	2.90E-02	-0.03
Cas.2	200	1.70E-02	1.50E-02	-0.12
Cas.3	10	7.70E-02	7.80E-02	0.01
Cas.3	80	5.50E-02	5.70E-02	0.04
Cas.3	140	3.10E-02	3.20E-02	0.03
Cas.3	200	1.90E-02	1.60E-02	-0.16

$$\mu = \begin{cases} \dfrac{\left(\left|\overrightarrow{R}_n\right| - \left|\overrightarrow{R}_{next}\right|\right)}{\left|\overrightarrow{R}_{10th}\right|}, & n = 10th, 80th, 140th \\ \dfrac{\left(\left|\overrightarrow{R}_{200th}\right| - 0\right)}{\left|\overrightarrow{R}_{10th}\right|}, & n = 200th. \end{cases} \quad (56)$$

R_{cab} is wave and x direction motion; R_{csw} is wave, x motion and RBSIBF;

Table 7: Calculation of acceleration reduction of each condition node relative to case 1.

Cas.	Node	Cab (m/s^2)	μ	Csw (m/s^2)	μ
Cas.1	10	9.70E-02	0.36	9.60E-02	0.34
Cas.1	80	6.20E-02	0.36	6.30E-02	0.36
Cas.1	140	2.70E-02	0.13	2.80E-02	0.18
Cas.1	200	1.40E-02	0.14	1.10E-02	0.11
Cas.2	10	8.70E-02	0.30	8.60E-02	0.27
Cas.2	80	6.10E-02	0.36	6.30E-02	0.40
Cas.2	140	3.00E-02	0.15	2.90E-02	0.16
Cas.2	200	1.70E-02	0.20	1.50E-02	0.17
Cas.3	10	7.70E-02	0.29	7.80E-02	0.27
Cas.3	80	5.50E-02	0.31	5.70E-02	0.32
Cas.3	140	3.10E-02	0.16	3.20E-02	0.21
Cas.3	200	1.90E-02	0.25	1.60E-02	0.21

R_{wave} is wave motion; R_{rbs} is RBSIBF; R_x is top x movement;

η is growth rate; μ is relative reduction.

Figures 18–21 show the calculation results of case 1. The reactions of nodes 10th-200th are 9.7E-02m/s^2, 6.2E-02m/s^2, 2.7E-02m/s^2, and 1.4E-02m/s^2. It presents structural transverse acceleration decreases affected by wave and in-line motion when the node number increases, as shown in Figure 26. With the depth increasing, SCR is weakened when affected by wave and in-line motion as shown in formula (25)-(26), and acceleration reaction is also reducing.

Along depth direction, the 10th-200th nodes' accelerations are reducing 0.36, 0.36, 0.13, and 0.14.

There are similar situations in cases 2 and 3. In a single case, the acceleration value decreases as the node number increases, as shown in Figures 26–28 and Table 8. From the perspective of multiple cases, the structural accelerations of node 10th-80th decrease as the case amplitude decreases, as shown in Figures 22 and 23, while the structural accelerations of node 140th-200th increase as shown in Figures 24 and 25 and 8 [19]. Table 9 gives the normalized values.

With the case number augmenting, top platform motion amplitude recedes while frequency increasing. The acceleration attenuation of nodes 10th-80th is positively correlated with the attenuation of top motion amplitude, and the acceleration increase of nodes 140th-200th is positively correlated with the increase of top motion frequency. The different region response is different, region's reaction during

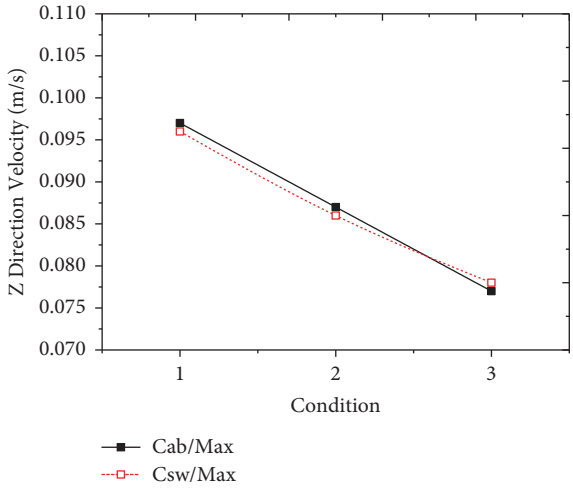

Figure 22: The 10th node structure acceleration response changing with cases.

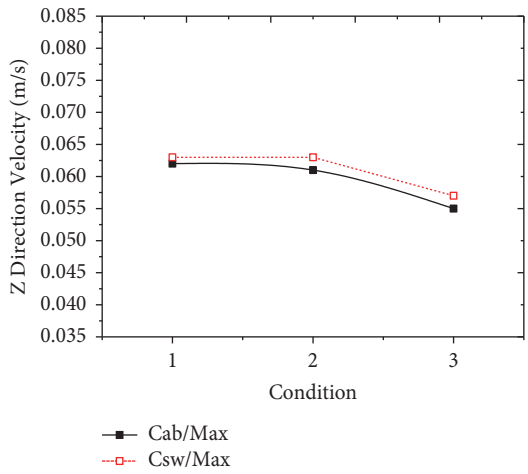

Figure 23: The 80th node structure acceleration response changing with cases.

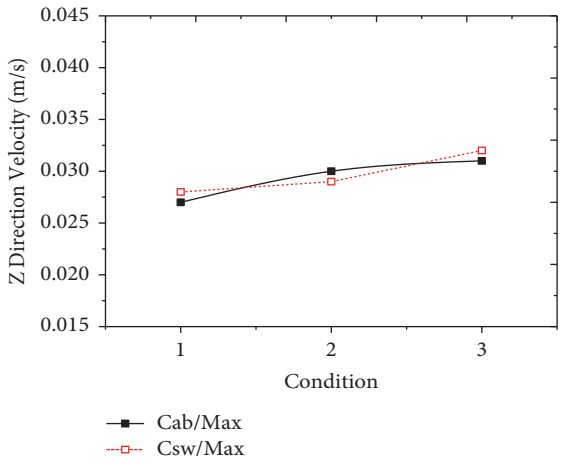

Figure 24: The 140th node structure acceleration response changing with cases.

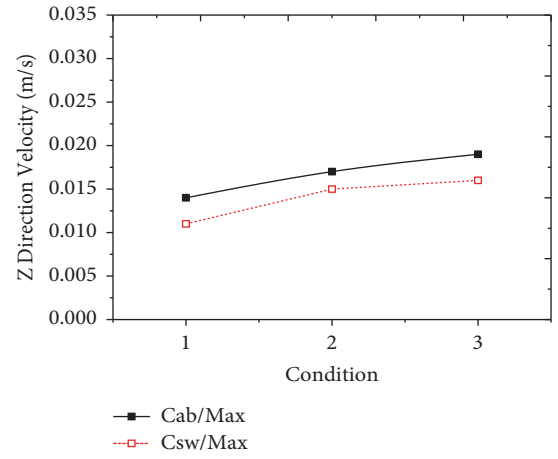

Figure 25: The 200th node structure acceleration response changing with cases.

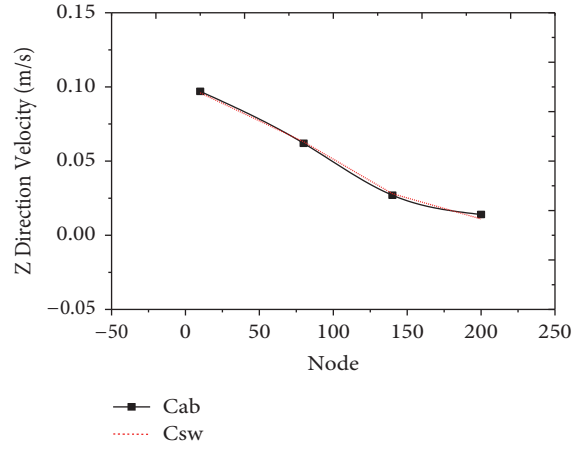

Figure 26: The acceleration reaction changes following node increasing in case 1.

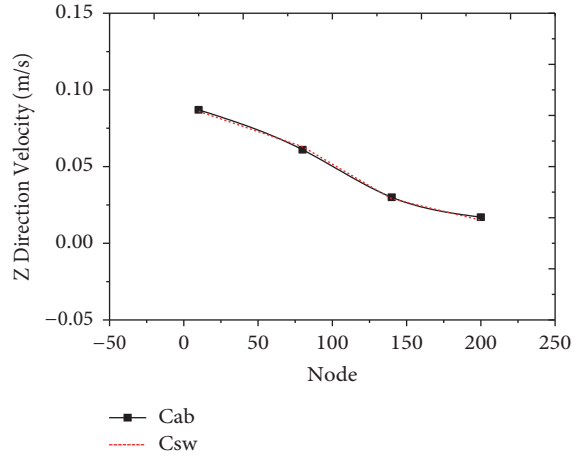

Figure 27: The acceleration reaction changes following node increasing in case 2.

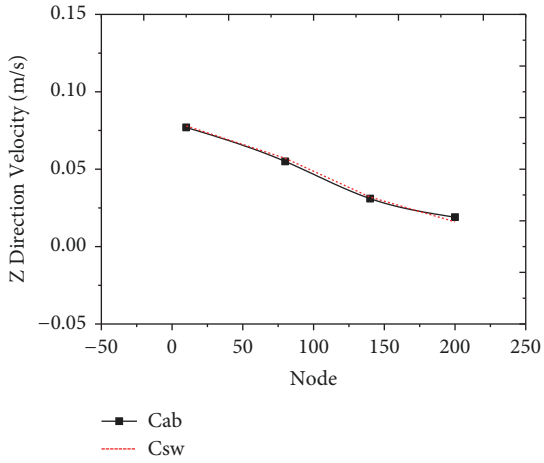

Figure 28: The acceleration reaction changes following node increasing in case 3.

10th-80th is significantly affected by the amplitude, and the response of node 140th-200th region is significantly affected by the frequency.

Enduring wave superimposed RBSIBF and top platform motion, 10th-200th reactions are 9.60E-02m/s^2, 6.30E-02m/s^2, 2.80E-02m/s^2, and 1.10E-02m/s^2, indicating cross-flow response recedes with depth, as presented in Figure 26. The effect of RBSIBF is weak and wave and top motion have higher influence than RBSIBF on reactions of structure.

Along node number increasing direction, accelerations of node 10th-200th reduce 0.34, 0.36, 0.18 and 0.11.

There are similar situations in case 2 and 3. In a single case, the acceleration value decreases as the node number increases, as shown in Figures 26–28 and Table 8. From the perspective of multiple cases, the structural acceleration of node 10th-80th decreases as the working condition amplitude decreases, as shown in Figures 22 and 23, while the structural acceleration of 140th-200th increases as shown in Figures 24 and 25 and 8.

With the case number augmenting, top platform motion amplitude recedes while frequency increasing. The attenuation of acceleration of 10th-80th node is positively correlated with the attenuation of top motion amplitude, and the increase of the acceleration of node 140th-200th is positively correlated with the increase of top motion frequency. The response of the structure is different at different nodes, the speed of node 10th-80th region is significantly affected by the amplitude, and the speed of node 140th-200th region was significantly affected by the frequency.

During node 10th-80th and 140th-200th, there is little influence on the change trend of regional acceleration with water depth and with cases.

In a word, the calculation results are as most same as that of no superimposed RBSIBF.

The load effect and load response of wave and its RBSIBF effect and top platform motion can be a linear expression. The amplitude change considering RBSIBF of node 10th-200th is -0.01, 0.02, 0.04, and -0.21. Frequency difference and phase difference exist in the RBSIBF, linear motion, and wave load, and the response is the increase, decrease, and even offset of amplitude.

In terms of the response increase of the structure, the increase of the calculation is not a factor to the structure. In addition to the value increase of the RBSIBF, reaction decreases with node number increasing, which also augments the percentage of the structure significantly. With the increase of water depth, when the structure rotates mainly in horizontal plane, the RBSIBF is positively correlated with the rotation vector diameter S. The RBSIBF increases acceleration reaction. When the structure rotates in surface vertical to flow direction, the RBSIBF reduce acceleration reaction of the structure. Other conditions are not significantly different, as presented in Tables 6 and 7.

As far as the structure is affected by the amplitude and frequency, RBSIBF increases the upper structure and weakens the lower reaction. RBSIBF upper is relatively weak and the structure suffering the wave is obvious. With node number augmenting, structural reaction reduces rapidly. The RBSIBF reaction is close to the order of magnitude of the structure response under wave and top motion, and the influence of the structure frequency is obvious.

In terms of three-dimensional response of the structure, as node coordinates increases, the rigid body response value in the 200th node increases the negative response of the structure. The reason is that the structure particles gradually develop from the narrow range oscillation in in-line direction of the 10th node to the 200th narrow range oscillation in vertical motion. The 200th motion in vertical motion reduces the response of RBSIBF. RBSIBF causes structural reaction under wave and top motion to be reduced. This is explained by the RBSIBF reaction to the structural response in a simple way.

It should be noted that as the water depth increases, each node's acceleration reaction decreases comparing to suspension node. Attenuation shows relatively severe in node 10th-80th, and the amplitude range is relatively weak in node 140th-200th.

In Figures 26–28, the swing in the top region is the largest; with the increase of node in each case, the swing gradually decreases. This trend is not significantly different from wave load. The response of top motion to structure decreases gradually with the increase of node number. The influence of boundary effect on structure accords with the basic understanding. The oscillation equation (16) can explain the structural response from the angle of single pendulum. The trend can also be used as part of the verification of calculations.

The normalization value in Table 8 may easily gain simulation case factor with respect to case one, which may give variation range under the influence of the case amplitude. While case amplitude lessens 0.5, the structural response decreases by 0.1-0.5.

As can be seen through comparing case 1-3 node 10th-200th and Figure 8, with amplitude diminution, 10th and 80th reaction reduces. The corresponding of node 140th and 200th has a tendency of increasing. 200th node is touch down node, and its RBSIBF amplitude and other nodes have difference. The bottom reaction which mainly moves in vertical direction

Table 8: Calculation of acceleration reduction.

Cas.	Node	Cab(m/s^2)	μ	Csw(m/s^2)	μ
Cas.1	10	9.70E-02	0.36	9.60E-02	0.34
Cas.2	10	8.70E-02	0.30	8.60E-02	0.27
Cas.3	10	7.70E-02	0.29	7.80E-02	0.27
Cas.1	80	6.20E-02	0.36	6.30E-02	0.36
Cas.2	80	6.10E-02	0.36	6.30E-02	0.40
Cas.3	80	5.50E-02	0.31	5.70E-02	0.32
Cas.1	140	2.70E-02	0.13	2.80E-02	0.18
Cas.2	140	3.00E-02	0.15	2.90E-02	0.16
Cas.3	140	3.10E-02	0.16	3.20E-02	0.21
Cas.1	200	1.40E-02	0.14	1.10E-02	0.11
Cas.2	200	1.70E-02	0.20	1.50E-02	0.17
Cas.3	200	1.90E-02	0.25	1.60E-02	0.21

Table 9: Acceleration normalized value with respect to case one.

Cas.	Node	Cab(m.s^2)	Normalized value	Csw(m.s^2)	Normalized value
Cas.1	10	9.70E-02	1.0E+00	9.60E-02	1.0E+00
Cas.2	10	8.70E-02	9.0E-01	8.60E-02	9.0E-01
Cas.3	10	7.70E-02	7.9E-01	7.80E-02	8.1E-01
Cas.1	80	6.20E-02	1.0E+00	6.30E-02	1.0E+00
Cas.2	80	6.10E-02	9.8E-01	6.30E-02	1.0E+00
Cas.3	80	5.50E-02	8.9E-01	5.70E-02	9.0E-01
Cas.1	140	2.70E-02	1.0E+00	2.80E-02	1.0E+00
Cas.2	140	3.00E-02	1.1E+00	2.90E-02	1.0E+00
Cas.3	140	3.10E-02	1.2E+00	3.20E-02	1.1E+00
Cas.1	200	1.40E-02	1.0E+00	1.10E-02	1.0E+00
Cas.2	200	1.70E-02	1.2E+00	1.50E-02	1.4E+00
Cas.3	200	1.90E-02	1.4E+00	1.60E-02	1.5E+00

may be a reason, while other nodes mainly move in in-line direction. Among the intermediate nodes, RBSIBF reaction is more than non-RBSIBF reaction, and it also increases or decreases. And since the motion frequency applied at the top is different from that of other loads, the response is a relatively random curve.

5. Conclusion

A little groundwork has been laid before and the response characteristics of RBSIBF have been studied. On the basis of Cable3D large deflection flexible beam, the fixed items have been replaced by iterative method, and the numerical iterative method has been revised. Orcaflex and experiment were used for comparative analysis. And the research shows that the calculation can be stable to a certain extent, close to the test and numerical simulation data, but there was a certain gap between the accuracy and the test, which needed to be further studied. Compared with the original method, the accuracy of the iterative method was not much different, and the search space increased. On the basis of large deflection beam, this paper considered the coupling of wave, platform movement and RBSIBF, and wave and top motion was input into the equation by load term. On this basis, Lissajous' figures verification and amplitude frequency curve had been used for verification, which had been proved by experiments. And also it was suitable for existing design to consider RBSIBF with a certain safety influence coefficient.

However, although a lot of work has been carried out before, there is still a long way to go before the calculation of multiple load terms; the Lissajous' figures check, the influence coefficient, and even the safety coefficient are given and truly applied to the marine riser design. A lot of work is still very superficial. In terms of transverse flow response, RBSIBF is only one of many influencing factors. These effects, such as wave load, vortex-induced vibration, and structural function layer due to load microadjustment, are from macro to microprocess. In these processes, some load items, such as wave and vortex-induced vibration, are more studied, and some load items, such as RBSIBF, are less studied. However, these cross-flow effects are real and should be given relatively high attention. So this paper also does some work on checking and influence coefficient.

In this paper, the effects of acceleration and frequency are analyzed. Based on the numerical model of the structure, the acceleration is analyzed along the water depth with or without RBSIBF. The effect of RBSIBF on structural

reaction is considered through the safety coefficient. The main conclusions of this paper are as follows.

The RBSIBF superposed on SCR is studied without considering flow, and other loads which have influence on the structure are simulated considering mutual effect.

(1) For overall motion, increasing along the node number, the structural response is no longer a simple graph. The motion response in xy plane develops gradually from the in-line narrow amplitude oscillations of hanging node region to the vertical narrow amplitude oscillations of bottom touchdown point region.

(2) From the perspective of influence of RBSIBF relative to other loads, structural transverse acceleration appears to decrease slowly with node number increasing under the action of loads. After coupling in-line movement, response attenuation with node number increasing persists. It indicates that in-line movement has no more influence on the structural acceleration than the wave load.

(3) Considering the RBSIBF effect on structural response, this article linear superposed the in-line direction motion. The structure response influence on the increase of acceleration response at the bottom touchdown area is not considered. The greatest influence point on the acceleration of RBSIBF is the 200th node and the acceleration is most affected by about 20%.

When the structure rotates mainly in the xz plane for node 10th-140th, RBSIBF is positively correlated to rotation vector diameter S. RBSIBF increases acceleration of structure. In the rotational yz plane of the structure node 200th, RBSIBF reduces acceleration reaction.

(4) In terms of the change of structure in depth direction, the top node region acceleration value decrease or attenuation range is more intense, while corresponding is relatively weak in the bottom region.

The response of the structural acceleration response of node 10th-80th region significantly reduces by about 30%. The acceleration attenuation of node 140th-200th is about 15%.

The acceleration of node 10th-80th decreases and the acceleration of node 140th-200th increases with the decrease of case amplitude.

The calculation results show that the wave frequency of the structure > in-line direction motion frequency > structure bending frequency (the second order)> RBSIBF frequency. Wave has no resonance with natural oscillation.

From above research, it can be summed that, under wave load, x motion, and RBSIBF, structural three-dimensional response is from x to y gradually along the depth. Through the process, structural acceleration decreases with the increasing water depth. The amplitude decreases most strongly or violently in the top suspension area. The RBSIBF effect is related to the radius vector S. Due to RBSIBF, in-line movement and wave existing phase, frequency, and amplitude difference, the amplitude of reaction increases, decreases, or even offsets and reaction synchronizes with movement frequency.

6. Study Data

The authors state that the data of this calculation are included.

6.1. Static Analysis of a Cable with the Bottom Presenting. 03/28/2000

(I) Global Constants

(a) Indexs

400	NODE	(# of nodes)
1	NELTYP	(# of different element types)
1	NSEG	(# of segments)
3	NDIM	(# of dimensions - 2 or 3)
1	JOB	(1 = static, 2 = dynamic)
1	JMOTN	(1 = sin. motion, 2 = input forced motion)
2	NCNSTR	(# of constrained nodes)
-1	NINTL	(1 = given initial guess, -1 = not given)
1	NITER	(1 = iteration, -1 = no iteration, when job = 2)
1	NUNIT	(1 = SI Unit, 2 = English Unit)

(b) Parameters

0.60000			relaxation
0.10000E-05	99		iteration accuracy, # iterations
0.00000	1000.00000	0.02000	begin time, end time & time step
1025.00000	865.00000	9.80650	mass density of water, fluid; gravity
-1100.00000	0.00000		bottom depth, fairlead depth
0.20000			bottom friction coefficient

(II) Element and Nodal Information

(a) Physical Properties for Each Element Type

2	bar(1) or beam(2) element:type 1
0.20700E+12	Young's mod
0.35484E-03 0.35484E-03 0.35484E-03	moment of inertia (I)
0.98980E-01 0.98980E-01 0.98980E-01	cross-section area (Af)
0.73062E-01 0.73062E-01 0.73062E-01	internal cavity area (Ai)
0.17750E+00 0.17750E+00 0.17750E+00	dist. to outermost fiber
0.20300E+03 0.20300E+03 0.20300E+03	mass of the rod per unit length
0.35500E+00 0.35500E+00 0.35500E+00	diameters for hydrodynamic forces
1.20000E+00 1.20000E+00 1.20000E+00	normal drag coefficient
0.00000E+00 0.00000E+00 0.00000E+00	tangential drag coefficient
0.10000E+01 0.10000E+01 0.10000E+01	normal added-mass coefficient
0.00000E+00 0.00000E+00 0.00000E+00	tangential added-mass coefficient
0.99491E+03 0.99491E+03 0.99491E+03	total buoyancy/unit length

(b) Connections between Nodes

2500.00000	1	1	400	segment length & type, 1st & last nodes

6.2. The Process for Formulas (42) to (45) and (49) to (51)

(1) Process for Formulas (42) to (45) (Formulas (57), (58), and (61)). Thank you very much for the expert's opinion. The expert's opinion is very good. The acceleration term of the original formula (57) is calculated at moment K-1 instead of moment K. Taylor quadratic expansion is carried out for the displacement term in formula (58) and one Taylor expansion is carried out for the velocity term in formula (61). And the Lagrangian term of formula (67) is substituted by the moment K-1.

In the above process, the acceleration term at time K is iteratively corrected for the displacement quadratic item in formula (58). The acceleration at time K and time K-1 are substituted into the iterative formula respectively to achieve partial iterative updating, and at the same time to produce subterms similar to the residual term. The same method is adopted for the velocity term of formula (61). Partial K-1 substitution is carried out for one Taylor expansion term at time K.

So when this substitution occurs, there's correspondence coefficients γ and β. These coefficients like relaxation factors are small and control the rate of iteration. Although the expression can meet the requirements of Taylor expansion and iterative update in theory, these factors are basically selected as zero in the practical program. In addition to the assumption that the acceleration term at K-1 and K moment of the acceleration is similar like formula (57), the iterative factor may cause nonconvergence of the calculation due to the iterative control, so the basic selection of the calculation γ and β are zero. And the final expression is formula ((64)-(67)).

Acceleration

$$\ddot{u}^{(K)} = \ddot{u}^{(K-1)} \tag{57}$$

Displacement

$$\begin{aligned} u^{(K)} &= u^{(K-1)} + \Delta t \dot{u}^{(K-1)} \\ &\quad + \Delta t^2 \left(\frac{1}{2} - \beta\right) \ddot{u}^{(K-1)} \\ &\quad + \Delta t^2 \beta \ddot{u}^{(K)} \\ &= u^{(K-1)} + \Delta t \dot{u}^{(K-1)} \\ &\quad + \frac{1}{2} \Delta t^2 \ddot{u}^{(K-1)} \\ &\quad + \Delta t^2 \beta \left(\ddot{u}^{(K)} - \ddot{u}^{(K-1)}\right) \end{aligned} \tag{58}$$

$$\Delta t^2 \beta \left(\ddot{u}^{(K)} - \ddot{u}^{(K-1)}\right) = 0 \tag{59}$$

$$\begin{aligned} u^{(K)} &= u^{(K-1)} + \Delta t \dot{u}^{(K-1)} \\ &\quad + \frac{1}{2} \Delta t^2 \ddot{u}^{(K-1)} \end{aligned} \tag{60}$$

Velocity

$$\begin{aligned}\dot{u}^{(K)} &= \dot{u}^{(K-1)} + \Delta t\left(1-\gamma\right)\ddot{u}^{(K-1)} \\ &\quad + \Delta t\gamma\ddot{u}^{(K)} \\ &= \dot{u}^{(K-1)} + \Delta t\ddot{u}^{(K-1)} \\ &\quad + \Delta t\gamma\left(\ddot{u}^{(K)} - \ddot{u}^{(K-1)}\right)\end{aligned} \tag{61}$$

$$\Delta t\gamma\left(\ddot{u}^{(K)} - \ddot{u}^{(K-1)}\right) = 0 \tag{62}$$

$$\dot{u}^{(K)} = \dot{u}^{(K-1)} + \Delta t\ddot{u}^{(K-1)} \tag{63}$$

Iterative Expression

$$\ddot{u}^{(K)} = \ddot{u}^{(K-1)} \tag{64}$$

$$u^{(K)} = u^{(K-1)} + \Delta t\dot{u}^{(K-1)} + \frac{1}{2}\Delta t^2\ddot{u}^{(K-1)} \tag{65}$$

$$\dot{u}^{(K)} = \dot{u}^{(K-1)} + \Delta t\ddot{u}^{(K-1)} \tag{66}$$

$$\widetilde{\lambda}^{(K)} = \widetilde{\lambda}^{(K-1)} \tag{67}$$

(2) Process for Formulas (49) to (51) (Formulas (69), (70), and (71)). In terms of Lissajous figure, the load in in-line direction and y direction satisfies the characteristics of harmonic motion, and they are perpendicular to each other. Then their equations can be expressed as formula (68) and formula (69). The arccosine function is solved in the above two perpendicular directions, and the expressions in the two directions are formula (70) and formula (71).

Then the y direction formula (71) is multiplied by m_1, and the in-line direction formula (70) is multiplied by m_2. When $m_2n_1 = m_1n_2$, formula (73) can be obtained. The above formula curve depends on coefficient $m_2n_1 = m_1n_2$ and $m_1\varphi_2 - m_2\varphi_1$. In this process, it is necessary to pay attention to the requirement that the loads are perpendicular to each other and satisfy the simple harmonic function. And also the frequency ratio meets a certain integer ratio, references available in (24)-(25).

X and Y Direction Motion

$$x = A_1\cos\left(2\pi n_1t + \varphi_1\right) \tag{68}$$

$$y = A_2\cos\left(2\pi n_2t + \varphi_2\right) \tag{69}$$

$$\arccos\left(\frac{x}{A_1}\right) = \pm\left(2\pi n_1t + \varphi_1 + 2k\pi\right) \tag{70}$$

$$\arccos\left(\frac{y}{A_2}\right) = \pm\left(2\pi n_2t + \varphi_2 + 2m\pi\right) \tag{71}$$

Frequency Requirement

$$m_2n_1 = m_1n_2 \tag{72}$$

Trajectory Equation

$$\begin{aligned}&\cos\left(m_1\arccos\frac{y}{A_2} \pm m_2\arccos\frac{x}{A_1}\right) = \cos\left(m_1 2\pi n_2t\right. \\ &\left.+ m_1\varphi_2 + 2mm_1\pi - 2\pi m_2n_1t - m_2\varphi_1 - 2km_2\pi\right) \\ &= \cos\left(m_1\varphi_2 + 2mm_1\pi - m_2\varphi_1 - 2km_2\pi\right) \\ &= \cos\left(m_1\varphi_2 - m_2\varphi_1 + 2\pi\left(mm_1 - km_2\right)\right) \\ &= \cos\left(m_1\varphi_2 - m_2\varphi_1\right)\end{aligned} \tag{73}$$

Thank you for expert opinion.

Data Availability

The data used to support the findings of this study are included within the article.

Conflicts of Interest

The authors declare that they have no conflicts of interest.

Acknowledgments

Thanks are due to National Natural Science Foundation of China (51239008), National Natural Science Foundation Key Project (51739010; 51679223), National Natural Science Foundation of China (51878315; 51508220), National Natural Science Foundation for Young Scholars of China (51809101), and Jiangsu State Grid Science and Technology Project under Grant no. FW201804007. Thanks are due to Professor Zhang Jun of TexasA&M University; Professor Weiping Huang of Ocean University of China; and Professors Sun Yaodong and Gu Bingwei of Jiansu Ocean University. The authors acknowledge all the help.

References

[1] J. Liu, *Study of Out-of-Plane Motion of SCRs with Rigid Swing*, Ocean University of China, Qingdao, China, 2013.

[2] Y. Komachi, S. Mazaheri, and M. R. Tabeshpour, "Wake and structure model for simulation of cross-flow/in-line vortex induced vibration of marine risers," *Journal of Vibroengineering*, vol. 20, no. 1, pp. 152–164, 2018.

[3] N. B. Khan, Z. Ibrahim, M. I. Khan, T. Hayat, and M. F. Javed, "VIV study of an elastically mounted cylinder having low mass-damping ratio using RANS model," *International Journal of Heat and Mass Transfer*, vol. 121, pp. 309–314, 2018.

[4] V. Domala and R. Sharma, "An experimental study on vortex-induced vibration response of marine riser with and without semi-submersible," *Proceedings of the Institution of Mechanical Engineers, Part M: Journal of Engineering for the Maritime Environment*, vol. 232, no. 2, pp. 176–198, 2018.

[5] Z. Pan, W. Cui, and Q. Miao, "Numerical simulation of vortex-induced vibration of a circular cylinder at low mass-damping using RANS code," *Journal of Fluids and Structures*, vol. 23, no. 1, pp. 23–37, 2007.

[6] K. Hong and U. H. Shah, "Vortex-induced vibrations and control of marine risers: a review," *Ocean Engineering*, vol. 152, pp. 300–315, 2018.

[7] H. Al-Jamal and C. Dalton, "Vortex induced vibrations using Large Eddy Simulation at a moderate Reynolds number," *Journal of Fluids and Structures*, vol. 19, no. 1, pp. 73–92, 2004.

[8] F. K. Alfosail, A. H. Nayfeh, and M. I. Younis, "A state space approach for the eigenvalue problem of marine risers," *Meccanica*, vol. 53, no. 4-5, pp. 747–757, 2018.

[9] L. Aguedal, D. Semmar, A. S. Berrouk, A. Azzi, and H. Oualli, "3D vortex structure investigation using Large Eddy Simulation of flow around a rotary oscillating circular cylinder," *European Journal of Mechanics - B/Fluids*, vol. 71, pp. 113–125, 2018.

[10] W. Yang, Z. Ai, X. Zhang, R. Gou, and X. Chang, "Nonlinear three-dimensional dynamics of a marine viscoelastic riser subjected to uniform flow," *Ocean Engineering*, vol. 149, pp. 38–52, 2018.

[11] M. Lou, W. Wu, and P. Chen, "Experimental study on vortex induced vibration of risers with fairing considering wake interference," *International Journal of Naval Architecture and Ocean Engineering*, vol. 9, no. 2, pp. 127–134, 2017.

[12] Z. Kang, W. Ni, L. Zhang, and G. Ma, "An experimental study on vortex induced motion of a tethered cylinder in uniform flow," *Ocean Engineering*, vol. 142, pp. 259–267, 2017.

[13] X. Wang, Z. Guan, Y. Xu, and Y. Tian, "Signal analysis of acoustic gas influx detection method at the bottom of marine riser in deepwater drilling," *Journal of Process Control*, vol. 66, pp. 23–38, 2018.

[14] F. Huera-Huarte, Z. Bangash, and L. González, "Towing tank experiments on the vortex-induced vibrations of low mass ratio long flexible cylinders," *Journal of Fluids and Structures*, vol. 48, pp. 81–92, 2014.

[15] Y. Hu, J. Cao, B. Yao, Z. Zeng, and L. Lian, "Dynamic behaviors of a marine riser with variable length during the installation of a subsea production tree," *Journal of Marine Science and Technology*, vol. 23, no. 2, pp. 378–388, 2018.

[16] N. Srinil, B. Ma, and L. Zhang, "Experimental investigation on in-plane/out-of-plane vortex-induced vibrations of curved cylinder in parallel and perpendicular flows," *Journal of Sound and Vibration*, vol. 421, pp. 275–299, 2018.

[17] M. M. Cicolin, B. Ma, and L. Zhang, "Experimental investigation on in-plane/out-of-plane vortex-induced vibrations of curved cylinder in parallel and perpendicular flows," *Applied Ocean Research*, vol. 65, pp. 290–301, 2017.

[18] FMCTechnologies.ExxonMobil(Exxon)Diana(DB/OL), 2018, http://www.fmctechnologies.com/en/SubseaSystems/Global-Projects/NorthAmerica/US/ExxonMobilDiana.aspx?tab=[9EBD9569-72A5-45E1-9928-1DAD94368B7A].

[19] X. Yao, *On the Dynamic Response and Fatigue of Steel Catenary Riser with Rigid Swinging*, Ocean University of China, Qingdao, China, 2018.

[20] W. Huang and X. Bai, *Structural Dynamics*, Modern Education, 2013.

[21] Y. Jx, "Study on the properties of Lissajous Figures," *Journal of Xihua University Natural Science*, vol. 27, no. 6, pp. 98–100+ 125, 2008.

[22] J. X. Yang, "Study on the synthesized path of two simple harmonic vibrations with one Vertical to another," *Journal of Xihua University Natural Science*, vol. 2, pp. 76–78+82+5, 2008.

[23] Y. Li, L. J. Qian, and Y. Cheng, "Investigation of the second-order hydrodynamic response of TLP wind turbine system," *The Ocean Engineering*, vol. 35, no. 3, pp. 52–58+111, 2017.

[24] S. C. Di, S. Y. Ji, and Y. Z. Xue, "Analysis of ship navigation in level ice-covered regions with discrete element method," *The Ocean Engineering*, vol. 35, no. 3, pp. 59–69, 2017.

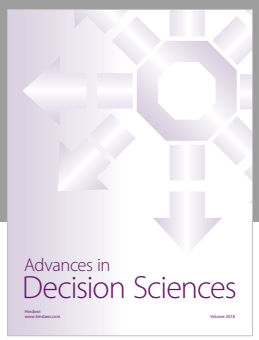

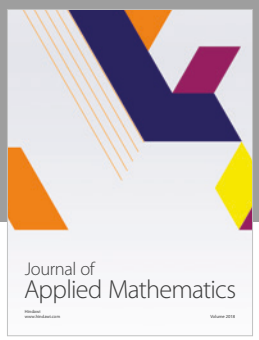

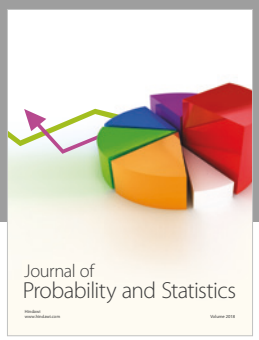

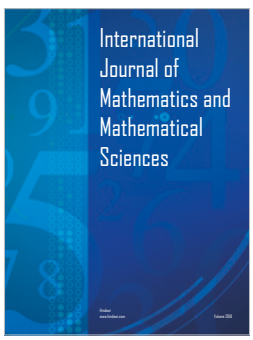

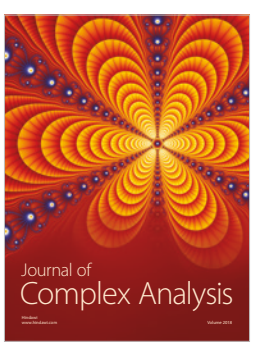

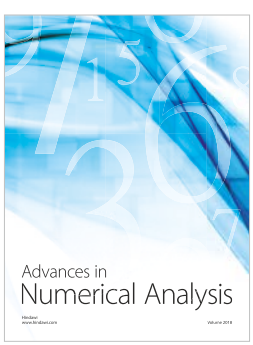

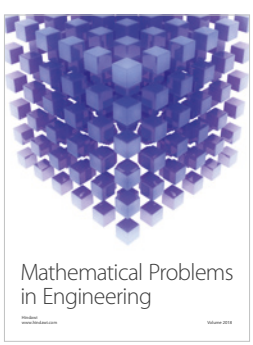

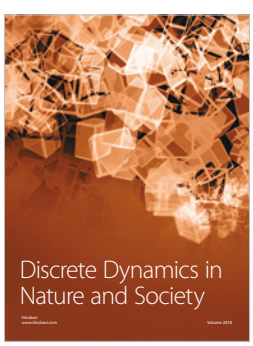

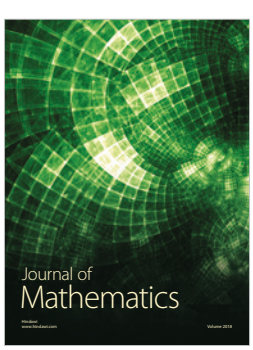

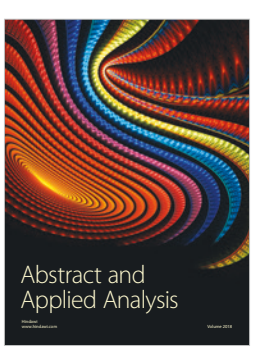

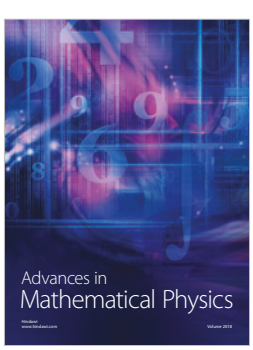

Hindawi

Submit your manuscripts at
www.hindawi.com